SUPPORTING INFORMATION

EXPERIMENTAL AND NUMERICAL INVESTIGATIONS OF EFFECTS OF SILICA COLLOIDS ON TRANSPORT OF STRONTIUM IN SATURATED SAND COLUMNS

Hesham M. Bekhit[1, ◊], Ahmed E. Hassan[1, 2, *], Rebekah Harris-Burr[1,3], and Charalambos Papelis[1, 4]

[1]Division of Hydrologic Sciences, Desert Research Institute, University System of Nevada, Las Vegas, NV 89119, USA

[2] Irrigation and Hydraulics Department, Faculty of Engineering, Cairo University, Giza 12613, Egypt

[3] Chemistry Department, University of Nevada Las Vegas, Las Vegas, NV 89154, USA

[4]Water Resources Management Graduate Program, University of Nevada Las Vegas, Las Vegas, NV 89154, USA

Total 12 pages including cover (5 Figures and 3 Tables)

SUMMARY

This section contains 3 tables covering a review of laboratory experiments for colloid and colloid-facilitated contaminant transport (Table S1), the physical properties of silica colloids used in the experiments (Table S2), and a summary of solution characteristics and experimental conditions for the ten column experiments (Table S3). It also contains a discussion of the Bromide breakthrough data and the associated modeling (Figure S1). Details of the mathematical model equations governing contaminant-colloid co-transport and the numerical solution to these governing equations (Figure S2) are also presented. In addition, modeling results and comparison to some of the experimental results are presented (Figures S3 through S5).

[◊]Present Address: Irrigation and Hydraulics Department, Faculty of Engineering, Cairo University, Giza 12613, Egypt.

[*] Corresponding Author: **Telephone**: 702-862-5465; **e-mail**: ahmed.hassan@dri.edu

Table S1. Review of laboratory experiments for colloid and colloid-facilitated contaminant transport.

Author	Column Length (cm)	Column Diameter (cm)	Colloid Type	Colloid Diameter (($\square$m)	Porous Media	Flow Velocity (cm/hr)	pH	Ionic Strength (M)	Solute.	Porous Media Particle Diameter(mm)
Corapcioglu and Choi (*1*)	30	2.5	latex colloid, sulfate latex	0.19-0.22	quartz sand	6	6.6			0.212-0.315
Grolimund (*2*)	12-Oct	1	clay	0.2	non calcareous soil	4	5 - 6	0.01-1	lead	1.0-2.0
Roy and Dzombak (*3*)	10	2.2	natural form of sand clay	0.468-1.0	sand	18.22	3.5-9	0.001, 0.01, 0.1	Ni^{2+} Phenanthrene	0.23-0.85
Luhrmann et al. (*4*)	50	5	Natural colloid	0.001-0.1	natural porous	0.198			$^{152}Eu_{III}$	0.2
Noell et al. (*5*)	50	0.635	amorphous Silica	0.1	saturated glass bed	6.3	8.9		cesium	0.42-0.36 0.15-0.21
Kretzschmar and Sticher (*6*)	Jun-45	1.0 or 2.5	hematite Fe_2O_3	0.15-0.1	acidic sandy soil	2-100	5.6-5.8			0.2-0.63
Saiers and Hornberger (*7*)	5.2	2.5	kaolinite	2	quartz sand	20	7.2	0.002-0.1	cesium	0.25-0.6
Sen (*8*)	30.5-27.9	2.5	kaolin	2.8	sand bed	27.8 & 122.4			Ni2+	0.69-0.85 0.178-0.105
Um and Papelis (*9*)	15	1.5	zeolitized tuf	0.45-10.0	zeolitized tuff	51.6 - 447	3.2-8.9	0.005-0.5	lead	
McCarthy et al. (*10*)	21	22	fluorescent carboxylate	0.1-0.5 1.0-2.1	fractures shale saprolite	0.6	4.4-5	0.1- 0.4, 1-15		

Table S2. Physical properties of silica colloids.

Property	Value
Surface functional groups	Si-OH
Mean diameter	0.97 μm (dynamic light scattering)
Density of solid polymer	1.96 g/mL
Number of microspheres per mL	2.093×10^{12}
Number of microspheres per gram*	1.068×10^{12}
Specific surface area◊	3.156 m^2/g

* Number of particles per gram of dry particles

◊ Provided by Bangs Laboratories, Inc.

Table S3. Summary of solution characteristics and experimental conditions for the ten column experiments.

Experiment	Chemical Conditions		Transport Properties			Initial Concentrations		Pulse Duration (pore volume)
	pH	Ionic strength, $NaNO_3$ (M)	V_x (cm/min)	D_L (cm^2/min)	Effective Porosity (θ)	Colloids (mg/L)	Strontium (M)	
Col_1	6.8	1.0×10^{-4}	1.80	0.095	0.35	100	0	4.7
Col_2	6.8	1.0×10^{-3}	1.80	0.095	0.35	100	0	4.6
Col_3	4.5	3.0×10^{-2}	2.02	0.106	0.35	100	0	9.0
Col_4	4.0	3.0×10^{-2}	2.10	0.110	0.35	100	0	4.3
Col_5	4.5	3.0×10^{-2}	2.02	0.106	0.35	0	1.0×10^{-5}	17.9
Col_6	4.0	3.0×10^{-2}	2.02	0.106	0.35	0	1.0×10^{-5}	18.3
Col_7	4.5	1.0×10^{-2}	1.80	0.095	0.35	0	1.0×10^{-5}	37.2
Col_8	6.8	1.0×10^{-3}	1.80	0.095	0.35	0	1.0×10^{-5}	75.6
Col_9	4.5	3.0×10^{-2}	2.02	0.106	0.35	100	1.0×10^{-5}	18.2
Col_10	4	3.0×10^{-2}	2.02	0.106	0.35	100	1.0×10^{-5}	18.5

Tracer Transport

A bromide solution having an initial concentration of 1.0 M was continuously injected into the column. Samples were collected from the effluent, the flow rate was calculated, and the concentrations of the effluent samples were measured. Once the concentration of Br in the effluent reached the inlet concentration, the injected solution was switched to NANOpure water, and the falling breakthrough was measured. The bromide concentrations were measured using a Br ion-selective electrode. A calibration of Br ion-selective electrode was conducted before measuring the Br concentration using the electrode. A calibration curve was prepared relating the electrode reading in mV to the natural logarithm of the Br concentration. The data were nicely fitted with a line and the regression coefficient, or coefficient of determination, R^2, was found to be about 0.987. Bromide transport in the sand column can be described as a one-dimensional, continuous injection into homogenous porous medium. The analytical solution to such a problem can be written as in literature cited (*11*)

$$\frac{C}{C_0} = 0.5\left[\operatorname{erfc}\left(\frac{L - V_x t}{2\sqrt{D_L t}}\right) - \exp\left(\frac{V_x L}{D_L}\right)\operatorname{erfc}\left(\frac{L + V_x t}{2\sqrt{D_L t}}\right)\right] \tag{S1}$$

where $\frac{C}{C_0}$ is the relative concentration at time t; L is the column height; D_L is the hydrodynamic dispersion coefficient parallel to the flow direction; V_x is the flow velocity in the column; and erfc is the complementary error function. A nonlinear, least-square optimization method (*12*) was used to obtain the transport properties (i.e., flow velocity and hydrodynamic dispersion coefficient). A comparison between one set of the experimental data and the analytical solution obtained using the best-fit values of V_x, and D_L is presented in Figure S1. These best-fit values are 20.27 mm/min for V_x and 10.65 mm^2/min for D_L. Once the flow velocity was estimated, the effective porosity was calculated by dividing the flow rate per unit area (specific discharge) by the velocity and was found to be 0.35.

Mathematical Model

Six coupled partial differential equations govern the processes involved in colloid-contaminant transport. These equations are described below and are based on literature cited (*13-15*).

$$\frac{\partial C_c}{\partial t} = \frac{\partial}{\partial x}\left(D_x \frac{\partial C_c}{\partial x} \right) - V\left(\frac{\partial C_c}{\partial x} \right) - K_1 C_c + \frac{K_2}{\theta} S_c \tag{S2}$$

$$\frac{1}{\theta}\frac{\partial S_c}{\partial t} = K_1 C_c - \frac{K_2}{\theta} S_c \tag{S3}$$

$$\frac{\partial (S_{cm} C_c)}{\partial t} = \frac{\partial}{\partial x}\left(D_x \frac{\partial (S_{cm} C_c)}{\partial x} \right) - V\left(\frac{\partial (S_{cm} C_c)}{\partial x} \right) + K_a C_f - K_{sm} S_{cm} C_c - K_1 S_{cm} C_c + \frac{K_2}{\theta} S_c S_{cc} \tag{S4}$$

$$\frac{1}{\theta}\frac{\partial (S_c S_{cc})}{\partial t} = K_a C_f - \frac{K_{sc}}{\theta} S_c S_{cc} + K_1 S_{cm} C_c - \frac{K_2}{\theta} S_c S_{cc} \tag{S5}$$

$$\frac{\partial C_f}{\partial t} + \frac{1}{\theta}\frac{\partial S_s}{\partial t} = \frac{\partial}{\partial x}\left(D_x \frac{\partial C_f}{\partial x} \right) - V\left(\frac{\partial C_f}{\partial x} \right) - 2K_a C_f + K_{sm} S_{cm} C_c + \frac{K_{sc}}{\theta} S_{cc} S_c \tag{S6}$$

$$\frac{1}{\theta}\frac{\partial S_s}{\partial t} = K_f C_f - \frac{K_r}{\theta} S_s = K_r \; K_d \; C_f - \frac{K_r}{\theta} S_s \tag{S7}$$

where each equation represents a mass balance equation for one of the six concentration variables that describe the transient conditions of the system. In the above equations, C_c represents the mass of mobile colloids per unit aqueous volume (ML^{-3}), S_c is the mass of captured colloids (immobile colloids) per unit total volume of porous media (ML^{-3}), S_{cm} is the mass of contaminant adhered to mobile colloids per unit mass of colloids (MM^{-1}), S_{cc} is the mass of contaminant adhered to immobile colloids per unit mass of colloids (MM^{-1}), C_f is the mass of dissolved contaminant per unit aqueous volume (ML^{-3}), S_s is the mass of contaminant sorbed onto solid matrix per unit total volume of porous media (ML^{-3}), θ is the porosity, D_x is the longitudinal dispersion coefficient (assumed to be the same for colloids and contaminant dispersion), V is the velocity (LT^{-1}), K_1 is the deposition rate coefficient of mobile colloids (T^{-1}), K_2 is the release rate coefficient of captured colloids (T^{-1}), K_a is the sorption (or attachment) rate coefficient of contaminant on mobile or immobile colloids (T^{-1}), K_{cm} is the release rate coefficient of contaminant from mobile colloids (T^{-1}), K_{sm} is the release rate coefficient of contaminant from the immobile colloids (T^{-1}), K_f is a forward (from liquid to solid matrix) reaction rate (T^{-1}) which is equivalent to the product (K_r K_d) with K_d being the distribution coefficient defining the apportioning of contaminant between the aqueous phase and the solid phase, and K_r is the backward reaction rate.

Numerical Model

The numerical model is formulated by discretizing the above equations using finite differences with a third order total variation diminishing (TVD) scheme (*16, 17*). This TVD solution is mass conservative and it does greatly reduce numerical dispersion and artificial oscillations. However, it adds a significant mathematical complexity to the discretization of the governing equations and increases the computational burden. The detailed description of the numerical model is presented in Bekhit and Hassan (*18*). Figure S2 displays a flowchart describing the solution to the six equations and the iterations involved in a single time step. Briefly, the discretization of the six equations results in three sets of linear systems of equations for Eqs. (S2), (S4), and (S6), with the other three equations solved by direct substitution. The linear systems are solved using a linear bi-conjugate gradient method (*19*). As a first step, equations (S2) and (S3) are solved together to get the concentration of the mobile and immobile colloids, C_c and S_c, respectively. The solution of these two equations is decoupled from the remaining four equations. The solutions of Eqs. (S4) to (S6) are complicated by the fact that they are coupled together and with the fully implicit scheme used here, they cannot be solved sequentially. Therefore, at any time step, an iterative solution algorithm is implemented where equations (S4) to (S6) are solved simultaneously and iteratively using previous time-step solutions until convergence is achieved. Once these equations are solved, C_f obtained from Eq. (S6) is substituted into Eq. (S7) to obtain S_s.

Colloid Transport Modeling: Experiments Col_2, Col_3, and Col_4

Figure S3a shows the results of the model fitting to experimental data from Col_2. The best-fit values for K_1 and K_2 are 3.33 hour^{-1} and 0.31 hour^{-1}, respectively. As shown in Figure S3a, a very good match between experimental data and the model is obtained for both the rising and falling portions of the breakthrough curve.

However, there is a noticeable scatter around the modeled breakthrough curves for high concentration values. As can be seen from the figure, the concentration of colloids quickly reaches 65% of the initial concentration then it starts to increase with a very small rate, which indicates that the deposition of some colloidal particles is irreversible (or that their release is very slow). These irreversible particles may cause the scattering in the colloid concentration around the high concentration values, as they may be released randomly and may have led to high concentration values in samples where these particles exist followed by lower values where such particles do not exist. The comparisons between experimental data from Col_3 and Col_4 and the model simulations are shown in Figure S4.

Strontium Transport Modeling: Experiment Col_7

The strontium transport in the sand column was found to be very sensitive to the ionic strength of the solution, and any small change in ionic strength would lead to a sudden change in the mobility of the strontium. The experiments discussed in the body of the paper (Col_5 and Col_6) were conducted under the same chemical conditions from the start to the end of the experiment. No change in solution pH or ionic strength was imposed during the experiment. However, it was of interest to explore the impact of a change in the chemical conditions on mobility of strontium. Experiment Col_7 was started with a solution having an ionic strength I = 1.0×10^{-2} M $NaNO_3$. After about 40 pore volumes and when the strontium concentration reached 85% of the initial concentration, the ionic strength of the solution was changed to 0.85×10^{-2} M $NaNO_3$. The results of the model fit to this experiment are shown in Figure S5. As can be seen from the experimental data, a change of the ionic strength from 1.0×10^{-2} M $NaNO_3$ to 0.85×10^{-2} M $NaNO_3$ causeed a sudden drop in the strontium concentration values. This sudden drop is attributed to the change in the sorption capacity of sand particles with the change in ionic strength.

In order to simulate this behavior, the distribution coefficient and reaction rate should be changed with changing the ionic strengths. Thus, to simulate this experiment, K_d and K_r are found to be 32 and 15 hour^{-1} with an ionic strength of 1.0×10^{-2} M $NaNO_3$, whereas their best-fit values become 74.07 and 0.81 hour^{-1} after changing the ionic strength to 0.85×10^{-2} M $NaNO_3$. As can be seen from Figure S5, the model successfully represents the rising breakthrough, the sudden drop in the breakthrough, and the falling breakthrough. In addition, the match between experimental data and model prediction is generally very good.

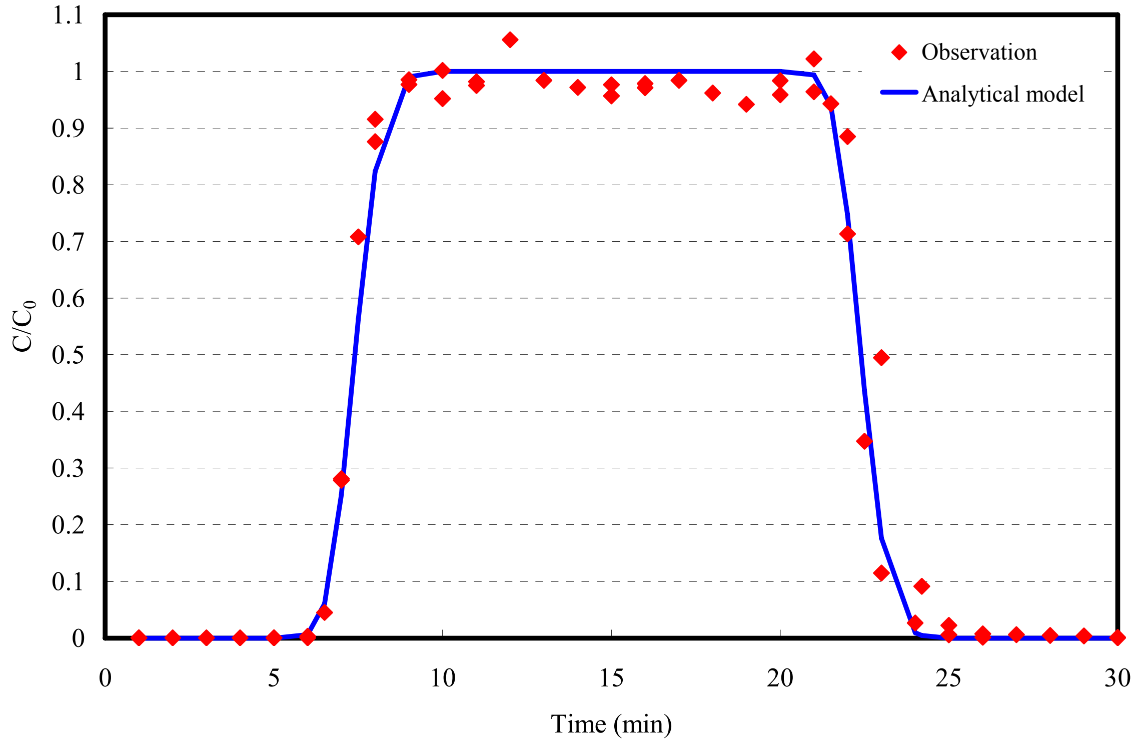

Figure S1. Comparison between raw data of rising and falling breakthrough curves for Br and analytical solution obtained with the best-fit parameter values.

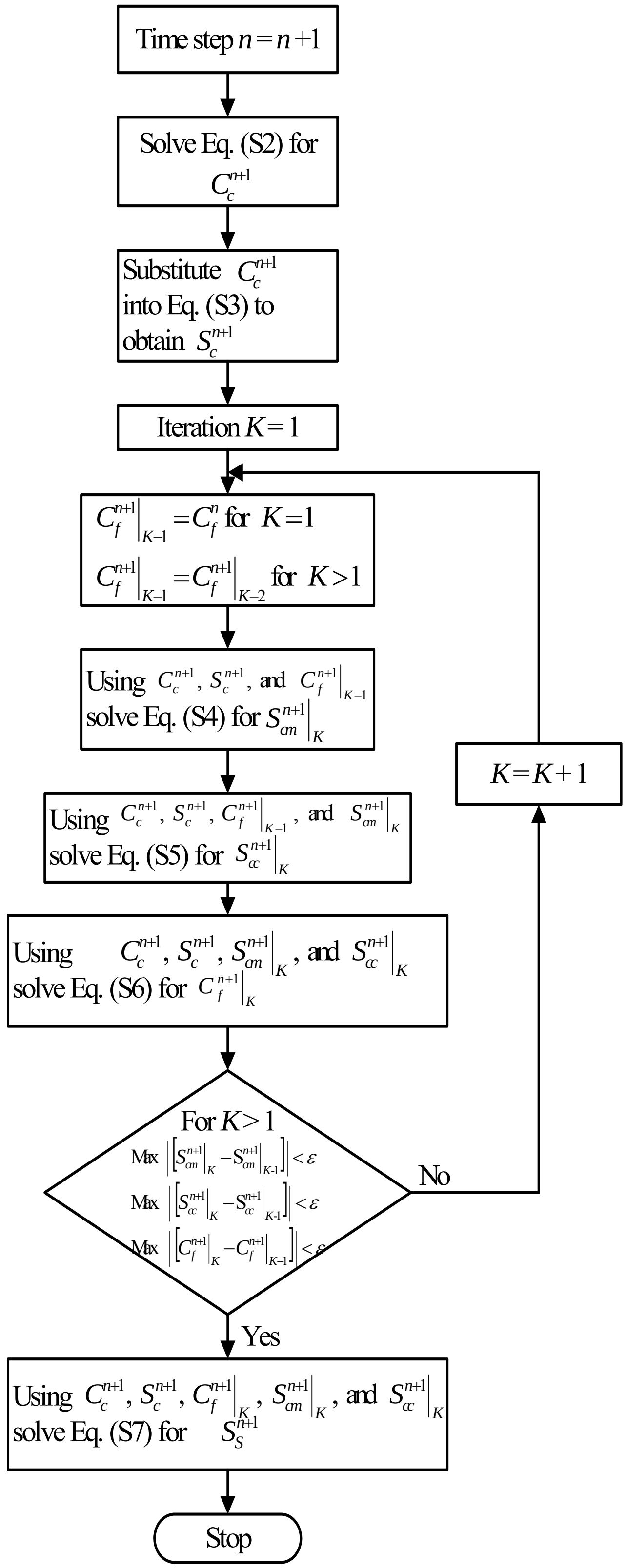

Figure S2. The steps of solving the six differential equations (Equations (S2) – (S7)) in one time step with the iterative solution of Equations (S4)-(S6) shown.

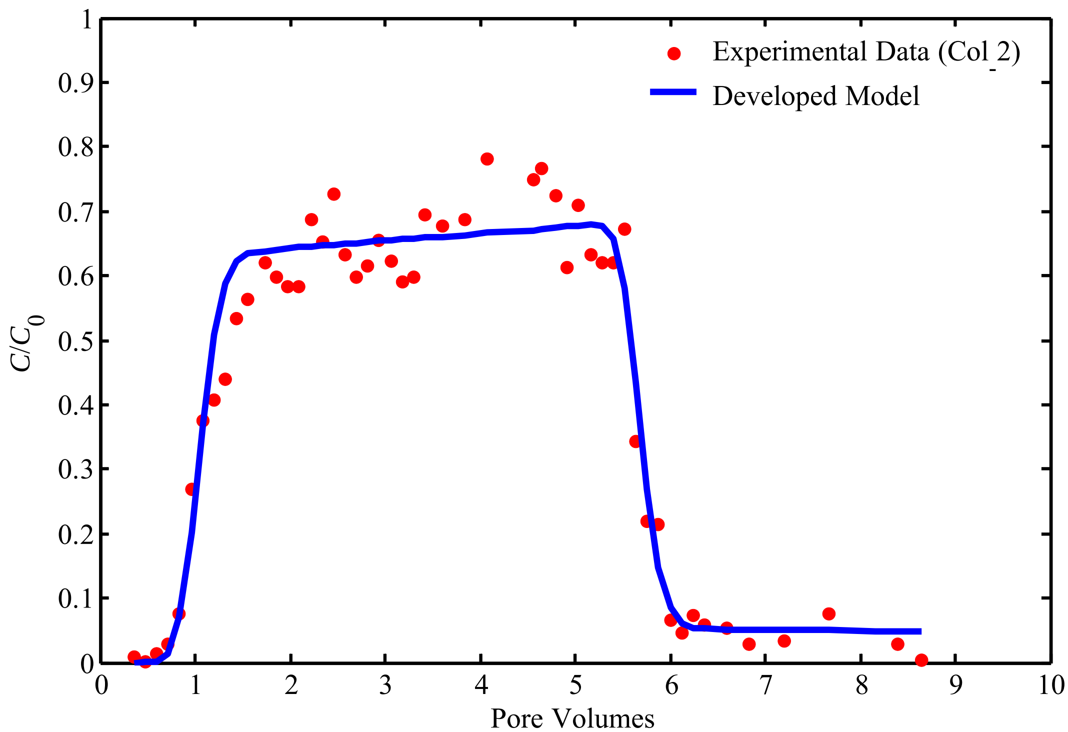

Figure S3. Comparison between the experimental data (Col_2) and the model results for the colloid breakthrough curves.

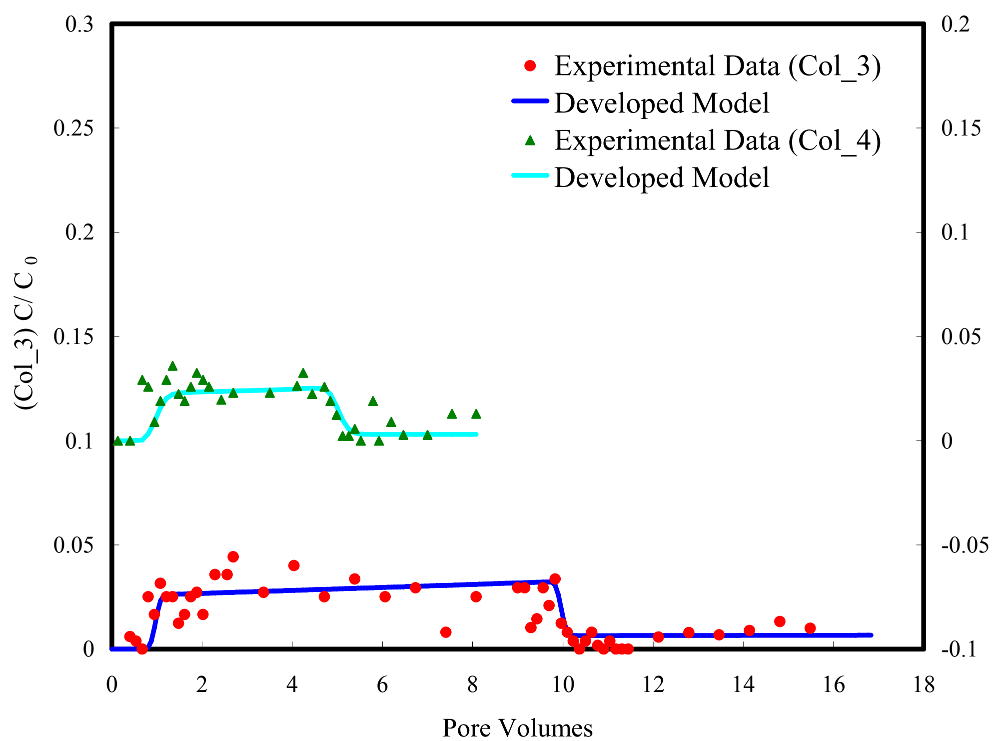

Figure S4. Comparison of colloid breakthrough curves as predicted from the model versus the experimental data from Col_3 and Col_4.

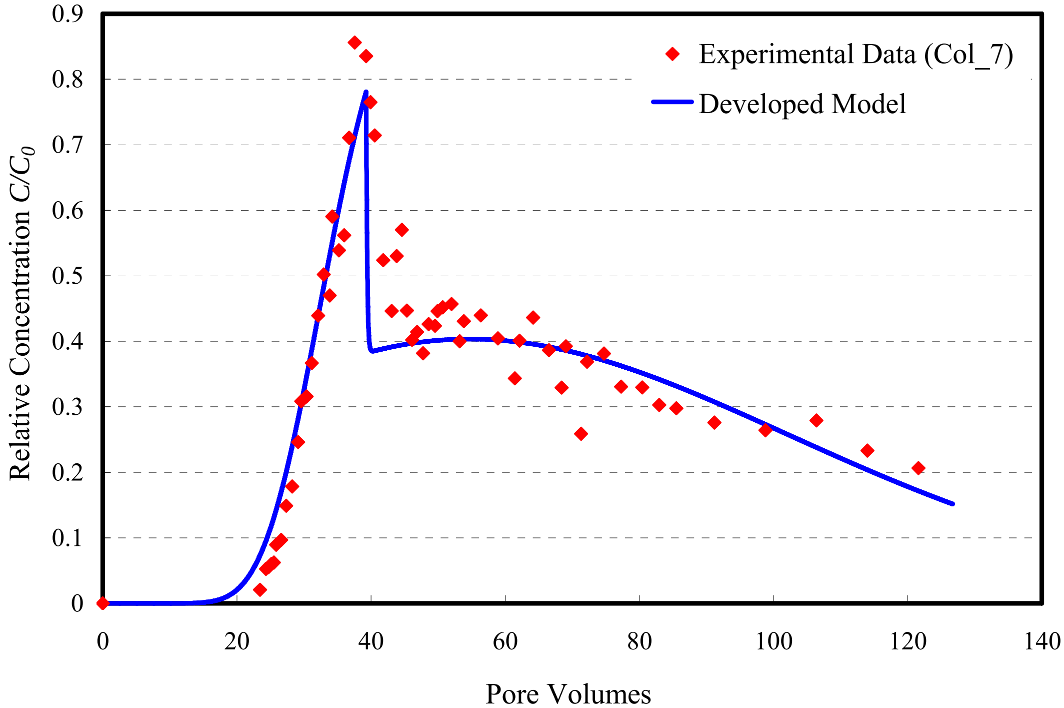

Figure S5. Comparison of strontium breakthrough curves as predicted from the model versus the experimental data from Col_7.

REFERENCES

(1) Corapcioglu, M. Y.; Choi, H. Modeling colloid transport in unsaturated porous media and validation with laboratory column data. *Water Resour. Res.* **1996**, *32*, 3437-3449.

(2) Grolimund, D.; Borkovec, M.; Barmettler, K.; Sticher, H. Colloid-facilitated transport of strongly sorbing contaminants in natural porous media: A laboratory column study. *Environ. Sci. Technol.* **1996**, *30*, 3118-3123.

(3) Roy, S. B.; Dzombak, D. A. Chemical factors influencing colloid-facilitated transport of contaminants in porous media. *Environ. Sci. Technol.* **1997**, *31*, 656-664.

(4) Luhrmann, L.; Noseck, U.; Tix, C. Model of contaminant transport in porous media in the presence of colloids applied to actinide migration in column experiments. *Water Resour. Res.* **1998**, *34*, 421-426.

(5) Noell, A. L.; Thompson, J. L.; Corapcioglu, M. Y.; Triay, I. R. The role of silica colloids on facilitated cesium transport through glass bead columns and modeling. *J. Contam. Hydrol.* **1998**, *31*, 1-2.

(6) Kretzschmar, R.; Sticher, H. Colloid transport in natural porous media; influence of surface chemistry and flow velocity. *Physics and Chemistry of the Earth* **1998**, *23*, 133-139.

(7) Saiers, J.; Hornberger, G. M. The role of colloidal kaolinite in the transport of cesium through laboratory sand columns. *Water Resour. Res.* **1996**, *32*, 33-41.

(8) Sen, T. K.; Mahajan, S. P.; Khilar, K. C. Colloid-associated contaminant transport in porous media: 1. Experimental studies. *AICHE Journal* **2002**, *48*, 2366-2374.

(9) Um, W.; Papelis, C. Geochemical effects on colloid-facilitated metal transport through zeolitized tuffs from the Nevada Test Site. *Environmental Geology* **2002**, *43*, 209-218.

(10) McCarthy, J. F.; McKay, L. D.; Bruner, D. D. Influence of ionic strength and cation charge on transport of colloidal particles in fractured shale saprolite. *Environ. Sci. Technol.* **2002**, *36*, 3735-3743.

(11) Ogata, A.; Banks, R. B. "A Solution of the Differential Equation of Longitudinal Dispersion in Porous Media," Professional Paper No. 411-A, USGS, Washington, DC. 1961.

(12) Toride, N.; Leij, F. J.; van Genuchten, M.T. "The CXTFIT Code for Estimating Transport Parameters from Laboratory or Field Tracer Experiments," U.S. Salinity Laboratory, USDA, ARS, Riverside, California, 1995.

(13) Corapcioglu, M. Y.; Kim, S. Modeling facilitated contaminant transport by mobile bacteria. *Water Resour. Res.* **1995**, *31*, 2639-2647.

(14) Corapcioglu, M. Y.; Jiang, S. Colloid-facilitated groundwater contaminant transport. *Water Resour. Res.* **1993**, *29*, 2215-2226.

(15) Kim, S.; Corapcioglu, M. Y. A kinetic approach to modeling mobile bacteria-facilitated groundwater contaminant transport. *Water Resour. Res.* **1996**, *32*, 321-331.

(16) Leonard, B. P.; Niknafs, H. S. Sharp monotonic resolution of discontinuities without clipping of narrow extrema. *Computer & Fluids* **1991**, *19*, 141-154.

(17) Zheng, C.; Wang, P. P. *MT3DMS: A modular three-dimensional multispecies transport model for simulation of advection, dispersion, and chemical reactions of contaminants in groundwater systems, documentation and user's guide*; U.S. Army Engineer Research Development Center Contract Report SERDP-99-1, Vicksburg, MS, 202p. 1999.

(18) Bekhit, H. M.; Hassan, A. E. Two-dimensional modeling of contaminant transport in porous media in the presence of colloids. *Advances in Water Resources* **2005**, *28*, 1320-1335.

(19) Press, W. H.; Teukolsky, S. A.; Vetterling, W. T.; Flannery, B. P. *Numerical Recipes in Fortran: The Art of Scientific Computing*; Cambridge University Press: New York, 1996.